RSC Sustainability

ROYAL SOCIETY OF CHEMISTRY

PAPER

View Article Online
View Journal | View Issue

Cite this: *RSC Sustainability*, 2025, **3**, 403

Solventless polyester synthesis using a recyclable biocatalyst magnetic nanoarchitecture†

Francesco Papatola,[a] Sawssen Slimani,[ab] Filippo Fabbri,[c] Georg M. Guebitz,[cd] Davide Peddis *[ab] and Alessandro Pellis *[a]

Received 28th August 2024
Accepted 19th November 2024

DOI: 10.1039/d4su00521j

rsc.li/rscsus

Improving enzyme activity and stability as well as preserving selectivity is a must for rendering biocatalysis an economically viable technology. These improvements can be achieved by immobilizing the biocatalyst on the surface of metal oxide magnetic nanoparticles. The aim of this work is to rational design Biocatalyst Magnetic Nanoarchitecture (BMN) consisting of spinel iron oxides nanoparticles having optimized morpho structural (*i.e.*, particles size, shape and crystallinity), textural (*i.e.*, high surface area) and magnetic properties. *Candida antarctica* lipase B (CaLB) was immobilized on the nanoparticles' surface investigating the optimal bioconjugation conditions and performing the biochemical characterizations to quantify protein concentration and to assess enzymatic activity. Once immobilized on the magnetic nanoparticles surface, CaLB was tested for an enzymatic polycondensation reaction to synthesize polyesters starting from renewable monomers such as the dimethyl ester of adipic acid and 1,8-octanediol. Conversion of monomers was >87% over three reaction cycles while the number average molecular weights of the products were between 4200 and 5600 Da with a dispersity <2. Efficient recycling of the enzyme upon magnetic separation was demonstrated for three reaction cycles.

Sustainability spotlight

The present study proposes enzymatic polymerization reactions to synthesize polyesters employing lipase (CaLB) covalently immobilized onto magnetic nanoparticles (*i.e.*, Biocatalyst Magnetic Nanoarchitecture). This ensures efficient recovery of the biocatalyst in environmentally friendly conditions (solventless) through the application of an external magnetic field facilitating its re-use over multiple polymerization cycles. This strategy was validated experimentally by carrying out the solvent-free polycondensation of dimethyl adipate and 1,8-octanediol and testing the preparation's recyclability over 3 reaction cycles. This work aligns with the following UN SDGs: 4-quality education, 9-industry, innovation and infrastructure and 12- responsible consumption and production.

1. Introduction

To satisfy the increasing request for biobased and biodegradable polymers, in line with the "European green deal",[1] the ability of enzymes to transform natural and non-natural compounds into polymers is considered as an environmentally friendly alternative to the traditional chemical synthetic pathways.[2] Biocatalysis is emerging as a fundamental tool within the chemical industry to produce pharmaceuticals and fine chemicals using mild and environmentally-friendly conditions.[3] Around the 1980s a new approach of polymer synthesis employing enzymes as catalysts has been developed, known as enzymatic polymerization.[4] In particular, enzymes from the class of hydrolases (*e.g.*, lipases, cutinases and esterases) are nowadays among the most commonly used biocatalysts for polyester synthesis since they are known for their versatility and thermostability.[5] Among these, the most widely used biocatalyst for the synthesis of polyesters is *Candida antarctica* lipase B (CaLB), due to its commercial availability both as free and immobilized catalyst.[6] However, enzyme applications are in most cases still limited due to the lack of long-term stability, difficult recovery and impossibility of re-use of the costly biocatalyst. These limitations could be overcome by utilizing enzyme immobilization strategies.[7,8] The immobilization of enzymes presents as the main objective to preserve and eventually enhance some of the enzyme's properties such as activity, stability and substrate specificity.[9] In addition, the immobilized preparations provide a tool for an easy separation of the biocatalyst from the reaction product facilitating its recovery and re-use. Biocatalysts costs and enzyme recyclability over several cycles of operation are in fact two of the main

[a]*Università di Genova, Dipartimento di Chimica e Chimica Industriale, Via Dodecaneso 31, Genova, 16146, Italy. E-mail: alessandro.pellis@unige.it; davide.peddis@unige.itmailto*

[b]*CNR, Istituto di Struttura della Materia, nM2-Lab, Monterotondo Scalo Roma, 00015, Italy*

[c]*Institute of Environmental Biotechnology, Department of Agrobiotechnology, IFA-Tulln, BOKU University, Konrad Lorenz Strasse 20, Tulln an der Donau 3430, Austria*

[d]*Austrian Centre of Industrial Biotechnology, Konrad Lorenz Strasse 20, Tulln an der Donau 3430, Austria*

† Electronic supplementary information (ESI) available. See DOI: https://doi.org/10.1039/d4su00521j

limiting steps for the cost-effective large scale implementation of enzyme-catalyzed reactions in the chemical industry.[10] In the last two decades, new promising strategies of enzyme immobilization were developed to further improve the separation of the biocatalyst from the reaction product. In particular, the field of nanotechnology has progressed significantly by leading to the fabrication and application of a wide range of nano-supports for the immobilization of enzymes and it is emerging as a general-purpose field having significant impact on catalysis.[11] Among them, magnetic nanoparticles (MNPs) have emerged due to their distinctive physico-chemical and magnetic properties. These MNPs possess several advantageous characteristics, including biodegradability, biocompatibility, low cost and the ability to be tailored with specific surface chemistries.[12] This immobilization strategy not only can provide an active and stable biocatalyst, but also it is a relatively simple and low-cost immobilization procedure that does not require an expensive support.[13] Some critical issues such as optimization of the magnetic properties, mass transfer limitations and low efficacy against insoluble substrates still need to be overcome. This very complex but promising scenario became an exciting playground where biotechnologist and materials physical chemist can produce novel biocatalyst magnetic nonarchitecture (BMN) by synergistic rational design of the magnetic and biocatalytic components.[14] The application of BMN represents a promising approach to enable the biocatalyst's immobilization satisfying both the need of preserving the enzyme's activity and the modern's day green chemistry principles that aim to follow the "do not significant harm" principle.[15,16] In fact, differently from other immobilization strategies based on non-magnetic carriers, their responsiveness to external magnetic field enables a rapid and efficient biocatalyst separation from reaction media simplifying significantly the purification steps in enzymatic reactions mainly by avoiding the use of organic solvents and other filtration systems. High surface to volume ratio, easy surface functionalization and peculiar magnetic properties (*i.e.*, superparamagnetism at room temperature, high saturation magnetization M_s), make MNPs an unique solid support for biocatalyst immobilization.[17] The main advantage of dealing with a superparamagnetic objects (*i.e.*, remanence magnetization and coercivity equal to zero) is that when the external magnetic field is removed, the magnetic object itself is not anymore magnetic. This will prevent clustering phenomena, and the presence of local magnetic fields. MNPs used as a support for enzyme immobilization have been successfully demonstrated in applications like substrate sensing,[18,19] immunoassays[20] and organic synthesis[21,22] and several studies have shown that the activity and stability of enzymes immobilized on MNPs are significantly better than unbounded enzymes[23,24] but without focusing on biocatalyst recycle system. Therefore, the overall intent of this study was to synthesize polyesters employing recyclable biocatalyst magnetic nanoarchitecture. Unlike other immobilization strategies where the recovery process in organic media could determine an irreversible activity reduction of the immobilized enzyme, the idea of the work was to recover biocatalyst without using any kind of solvents, but just a magnetic device, to exploit enzyme recyclability over multiple reaction cycles thanks to the retainment of its activity.

According to the literature,[25–27] for which CaLB exploits excellent selectivity towards long chain diols and acids, enzyme bound nanoparticles were tested for enzymatic polymerization reactions to synthesize polyesters starting from renewable monomers such as dimethyl adipate and 1,8-octanediol studying the preparation's recyclability over 3 cycles of reaction.

2. Experimental

2.1 Materials and methods

The chemicals $FeCl_2 \cdot 4H_2O$ (>99%), $FeCl_3 \cdot 6H_2O$ (>99%), HCl (98%), ammonium hydroxide (30%), ethanol (≥99.8%) dimethyl adipate (DMA, >99%), 1,8-octanediol (ODO, >99%), chloroform (99.0–99.4%), 2-methyl-2-butanol (>99%), 4-nitrophenol (>99%), *para*-nitrophenyl butyrate (*p*-NPB), bovine serum albumin (BSA), K_2HPO_4 (>98%) and KH_2PO_4 (>98%), lipase from *Candida* sp.(L3170) and *N*-(3-dimethylaminopropyl)-*N*-ethylcarbodiimide-hydrochloride (EDC) were purchased from Sigma-Aldrich.

MNPs synthesis. Spinel iron oxide nanoparticles were synthesized by the co-precipitation method using an aqueous solution of Fe^{2+} and Fe^{3+} with the stoichiometric ratio 1 : 2, by alkalization with 30% ammonia solution. The synthesis was done according to the following operating procedure: at 60 °C, a mixture of $FeCl_3 \cdot 6H_2O$ (>99%, Sigma-Aldrich) and $FeCl_2 \cdot 4H_2O$ (>99%, obtained from Sigma Aldrich) was dissolved in 100 mL 0.01 M HCl solution (obtained from Sigma Aldrich, 98%). The solution was alkalinized with 30% ammonium hydroxide. After two hours of magnetic stirring, the resulting precipitate was washed with deionized water for 3 cycles assisted by centrifugation, and adjusting the pH it was possible to obtain stable ferrofluids. The obtained black powders were dried overnight in an oven at 60–70 °C before further use.[28]

2.2 Characterization of MNPs

The crystalline structure was characterized by X-ray diffraction (XRD) measurements, using a TT 3003 diffractometer equipped with a secondary graphite monochromator, employing CuKα radiation ($\lambda = 1.5418$ Å). Data were collected in the 10–90° 2ϑ range with a step size of 0.04° and counting 4 s per step. A vibrating sample magnetometer (VSM Model 10–Microsense) equipped with an electromagnet producing a magnetic field in a range from −2 to +2 T was used to investigate the field dependence of magnetization.

Transmission electron microscopy (TEM) analysis was performed by using a Philips CM200 microscope operating at 200 kV and equipped with a LaB_6 filament. For TEM observations, the samples, in the form of powder, were prepared by using the following procedure. A small quantity of powder was dispersed in ethanol and subjected to ultrasonic agitation for ∼1 min. A drop of the suspension was deposited on a commercial TEM grid covered with a thin carbon film. Finally, the grid was kept in air until complete ethanol evaporation.

The Quantum Design PPMS (Physical Property Measurement System) magnetometer was utilized to investigate the magnetic properties of the samples. These samples, in powder form, were secured in polycarbonate capsules with epoxy resin to prevent particle movement during measurements. Field dependence of magnetization measurements were recorded at 5 K and 300 K. The thermal dependence of magnetization was measured using zero field-cooled (ZFC) and field-cooled (FC) protocols. For the ZFC measurements, the sample was first cooled in the absence of a magnetic field, and then the magnetization was measured during warming the sample in an applied field of 2.5 mT. For the FC measurements, the sample was cooled while maintaining the applied field of 2.5 mT, and magnetization was measured during the subsequent warming process keeping the field applied. The field dependence of remanent magnetization was investigated using the IRM (isothermal remanent magnetization) and DCD (direct current demagnetization) protocols. The IRM protocol begins with a demagnetized sample. A small positive magnetic field (H_{rev}) is applied, then removed, and the remanence (M_{IRM}) is measured in zero field. This process is repeated with increasing applied fields until the remanence reaches saturation. In the DCD measurement, the sample has been saturated in a positive direction. Then, a small negative magnetic field opposite to the magnetization direction is applied for a few seconds, then switched off, and the remanence (M_{DCD}) is measured. This process is repeated with increasing magnetic fields until the remanent magnetization reaches saturation. All the magnetic measurements were normalized by the mass of the magnetic phase. Saturation magnetization value (M_s) was determined from the portion at high field of M=(H) curves using as approach to saturation law (LAS).[29]

Immobilization of lipase on MNPs. After the synthesis of magnetic nanoparticles, *Candida antarctica* lipase B (CaLB) was immobilized onto the surface. The immobilization procedure was based on the formation of covalent bonds between the functional groups present on magnetic nanoparticles and on the enzyme protein upon carbodiimide- EDC activation. Therefore, in a glass vial, 250 mg of magnetic nanoparticles (MNPs) were weighted using an analytical balance. MNPs were added to 2 mL of buffer A (0.003 M KH_2PO_4/K_2HPO_4, pH 6). The reaction mixture was agitated for 10 min with a blood rotator (SB3 model from VWR) after adding 0.5 mL of EDC carbodiimide solution (0.025 g mL^{-1} in buffer A). Then, 2.5 mL of CaLB (lipase from *Candida* sp., obtained from Sigma Aldrich, L3170, 7.1 mg mL^{-1}), prepared by mixing 0.7 mL of enzymatic stock with 1.8 mL of buffer A (KH_2PO_4/K_2HPO_4, pH 6), was added and the reaction mixture was agitated for 24 h at RT with the rotator set at a speed of 40 rpm. Lipase-bound magnetic nanoparticles were recovered from the reaction mixture by placing the glass vial on a permanent magnet. The magnetic particles settled within 30 seconds and the supernatant was used for protein analysis while the precipitates were washed one time with buffer A and then buffer B (0.1 M K_2HPO_4/KH_2PO_4 pH 8.0). The binding of lipase onto the MNPs was confirmed using FT-IR (Shimadzu IRPrestige-21, equipped with a Specac golden gate single reflection diamond attenuated total reflection). All samples were analyzed in the 4000−600 cm^{-1} region and Fourier Transform was used as a data-processing technique.

The thermal stability of magnetic nanoparticles before and after enzyme immobilization was determined through a Thermogravimetric (TG) analysis by means of a Mettler Toledo micro and ultra-micro balances with sub-microgram resolution over the whole measurement range. Each sample (80 mg) was measured under air atmosphere and heated from 20 to 800 °C at a heating rate of 20 °C min^{-1}.

Esterase activity assay. The esterase activity of CaLB activity was determined by monitoring hydrolysis *para*-nitrophenyl butyrate (*p*-NPB) (Fig. S2†). The catalytic activity, which corresponds to the increment of the absorbance at 405 nm due to the hydrolytic release of *p*-nitrophenol (ε 405 nm), was monitored over 5 min in cycles of 30 s with a Tecan Plate Reader (Tecan, Grödig, Austria) using 96-well microtiter plates (Greiner 96 Flat Bottom Transparent Polystyrene).

Different enzymes dilutions were prepared using K_2HPO_4/KH_2PO_4 buffer pH 8, 0.1 M. Solution A consisting of 86 μL of *p*-NPB (*p*-nitrophenyl butyrate) and 1 mL of 2-methyl-2-butanol was prepared and stored at −20 °C until usage. Solution B was freshly prepared each time by mixing 160 μL of solution A and 4 mL of buffer (K_2HPO_4/KH_2PO_4 buffer 0.1 M pH 8). 200 μL of the solution B was mixed with 20 μL of the enzyme diluted in buffer. The samples were analyzed in triplicates and a series of blanks (*i.e.*, buffer without enzyme) were included in each activity cycle. The activity was calculated in units (U), where 1 unit is defined as the amount of enzyme required to hydrolyze 1 μmol of substrate per minute.

Protein concentration determination. To evaluate the efficiency of the immobilization procedure the protein concentration of the supernatant was determined using the Bio-Rad solution (Coomassie brilliant blue G-250 dye) and different solutions of BSA (Bovine Serum Albumin protein standard, 2 mg mL^{-1}, Sigma-Aldrich) as standard protein to obtain the calibration curve (Fig. S3†). The concentrations used were: 0.025, 0.03125, 0.0625, 0.1, 0.125, 0.2, 0.25, 0.5 and 1 mg mL^{-1}. Samples were diluted in 0.1 M K_2HPO_4/KH_2PO_4 buffer at pH 8 buffer while the dye was diluted 1 : 5 in mQ water. BioRad assay is based on the color change of Coomassie brilliant blue G-250 dye in response to various concentrations of protein (Fig. S4†). Absorbance was measured at 595 nm (ε protein–dye complex) over 5 min in cycles of 18 s with a Tecan Plate Reader (Tecan, Grödig, Austria) using a 96-well microtiter plate (Greiner 96 Flat Bottom Transparent Polystyrene) where 10 μL of each sample (in triplicate) and then 200 μL of BioRad solution was added to each pot. Incubation was performed at 400 rpm for 5 minutes at RT.

Enzymatic synthesis of polyesters. Enzymatic polymerization *via* polycondensation of dimethyl adipate and 1,8-octanediol was performed in bulk (*i.e.*, solvent-less) condition to be as environmentally friendly as possible using the MNP immobilized lipase as biocatalyst. Equimolar amounts of the two monomers (0.003 mol) and 10% w w^{-1} of the immobilized enzyme calculated on the total amount of the monomers were left to react at 85 °C for 6 h. After this time, pressure was reduced at 12 mbar for 18 h to remove the by-product, MeOH, that was formed during the reaction. The samples were then

analyzed *via* Proton Nuclear Magnetic Resonance (^{1}H-NMR) and Gel Permeation Chromatography (GPC) to determine the monomers conversion and the obtained molecular weights.

Characterization of the polyesters: proton nuclear magnetic resonance (^{1}H-NMR) and gel permeation chromatography (GPC). All ^{1}H-NMR spectra were recorded using a JEOL ECZ400R/S3 at a frequency of 400 MHz using $CDCl_3$ as the solvent. Gel permeation chromatography was performed at 30 °C on an Agilent Technologies HPLC System (Agilent Technologies 1260 Infinity) connected to a 17 369 6.0 mm ID × 40 mm L HHR-H, 5 μm Guard column and a 18 055 7.8 mm ID × 300 mm L GMHHR-N, 5 μm TSK gel liquid chromatography column (Tosoh Bioscience, Tessenderlo, Belgium) using THF as an eluent (at a flow rate of 1 mL min^{-1}). An Agilent Technologies G1362A refractive index detector was employed for detection. The molecular weights of the polymers were calculated using polystyrene calibration standards (250–70 000 Da) purchased from Sigma-Aldrich.

3. Result and discussions

3.1 Biocatalyst magnetic nanoarchitecture

CaLB was immobilized on MNPs using 2% of biocatalyst based on the amount of solid support. For several time-points (after 1, 2, 4, 8 and 24 h), the decrease of the free enzyme activity in the supernatant due to the immobilization onto magnetic nanoparticles is shown in Fig. 1A. Results for the protein concentration determination are also presented as residual protein concentration (%) for the same time-points (Fig. 1B). The immobilization results obtained using the lipase B from *Candida antarctica* (CaLB) show that after 24 h of immobilization of CaLB, 59% of the biocatalyst was successfully bound to the magnetic nanoparticles according to the esterase activity assay. This corresponds very well to 55% bound according to the decrease of the protein concentration in the supernatant (Fig. 1A and B respectively). As visible from the graphs, after 8 h of immobilization of CaLB, <50% of both the residual activity and concentration was detected in the supernatant by showing similar results to those observed after 24 h of immobilization. This could be explained by the fact that magnetic nanoparticle' surface sites were almost completely saturated after approximately 8 h. It is also worth to mention that, in presence of applied magnetic field a significant enhancement in the enzymatic activity can further observed, due to the influence of the magnetic field on the orientation and mobility of the immobilized enzymes. This has been recently proved in a study reported by Wang *et al.*,[30] showing that the application of magnetic field increased the catalytic activity of immobilized CaLB enzymes. This opens interesting perspectives on the role of magnetic nanoparticles and magnetic fields in influencing enzyme activity.

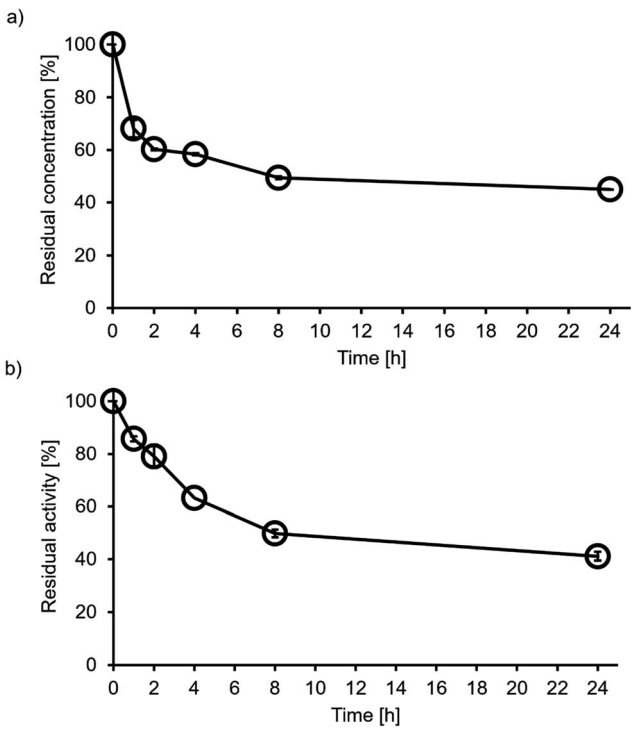

Fig. 1 Immobilization of CaLB onto MNPs. Graphical illustration of remaining protein concentration (a) and *para*-nitrophenyl butyrate activity (b) of the different timepoint supernatants for CaLB concentration of 2%.

Morpho-structural and magnetic properties of the bare (MNPs) and enzyme-functionalized nanoparticles (BMN) were investigated by X-ray diffraction, FT-IR and magnetometry. The X-ray diffraction patterns (Fig. 2a) show for both samples reflections typical of iron oxide phase with spinel structure (JCPDS card No. 75-449). Any extra phase has been detected and average crystallite size of 9.0 (1) nm was estimated for both samples by the Scherrer equation.[31] It is important to underline that XRD clearly indicated that functionalization process do not induce any relevant structural change in MNPs. To verify the immobilization of CaLB on MNPs surface, FT-IR analysis was performed on bare MNPs, pure CaLB and BMN (Fig. 2b). The characteristic absorption band of CaLB associated with the σ-type C–O (typical of aa residues) is present in CaLB bound MNPs at around 1036 cm^{-1} but is not present in bare MNPs confirming the binding of lipase to the nanoparticles. In addition to the characteristic σ-type C–O absorption band,[32] the IR analysis reveals the amide I bond transitions at 1630 cm^{-1}, related to the stretching vibrations of C=O groups and amide II band at 1540 cm^{-1}, due to the N–H bending. In the CaLB spectrum, the amide II transition is obscured by the O–H absorption, and it could be explained by the fact that enzyme was analyzed in water solution. However, in the BMN spectrum, both amide I and amide II transitions are visible. After CaLB immobilization, the absorption peak at 1630 cm^{-1} broadens and shifts, due to the overlapping with O–H bending from MNPs surface (*i.e.*, hydroxyl group). Additionally, the amide II region becomes more evident as the presence of a shoulder in the BMN spectrum absent in bare MNPs. These results support the bonding between the enzyme and the magnetic nanoparticles. Furthermore, as reported in the literature,[33,34] CaLB immobilization could occur through the –NH_2 functional groups of the enzyme onto modified surface of solid support. Nevertheless, since the EDC conjugation chemistry was used, we suppose a reaction

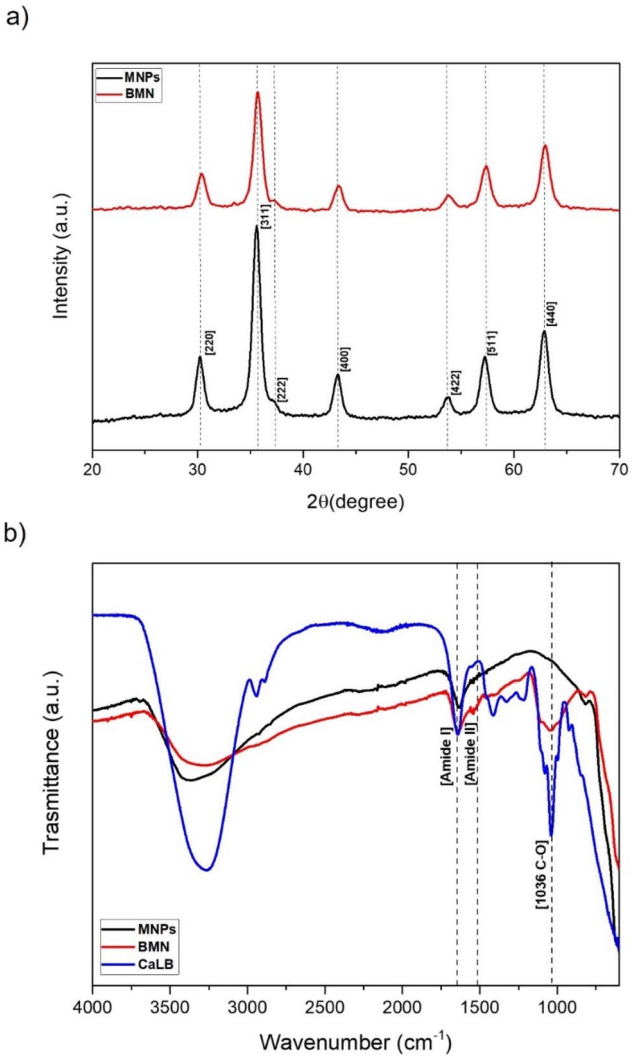

Fig. 2 (a) XRD pattern of MNPS (black) and BMN (red); (b) FT-IR of bare MNPs (black), BMN (red) and pure CaLB (blue).

between $-NH_2$ groups, formed from the use of concentrated ammonia solution on MNPs surface (as visible from the jagged behaviour of MNPs from 3500–2900 cm^{-1}), and carboxylic groups of the enzyme. A more detailed discussion on the grafting mode of CaLB on MNPs through the EDC bio-conjugation process is reported in ESI (Fig. S5)† as well as TGA analysis of MNPs before and after CaLB immobilization (Fig. S6†).

The typical TEM micrographs (Fig. S7†) for the bare MNPs show the presence of particles with mean particle size of 10 nm, confirming the XRD results.[28]

To study the effect of CaLB functionalization, a comparative magnetic investigation was carried out on both MNPs and BMN samples. Temperature dependence of magnetization measured by ZFC-FC protocols (Fig. 3a) exhibit for both samples typical behavior of an assembly of interacting single-domain particles.[35] The temperature corresponding to the maximum in the ZFC curve, T_{max}, is directly proportional to the average blocking temperature ($\langle T_b \rangle$) and was found to be the same for both

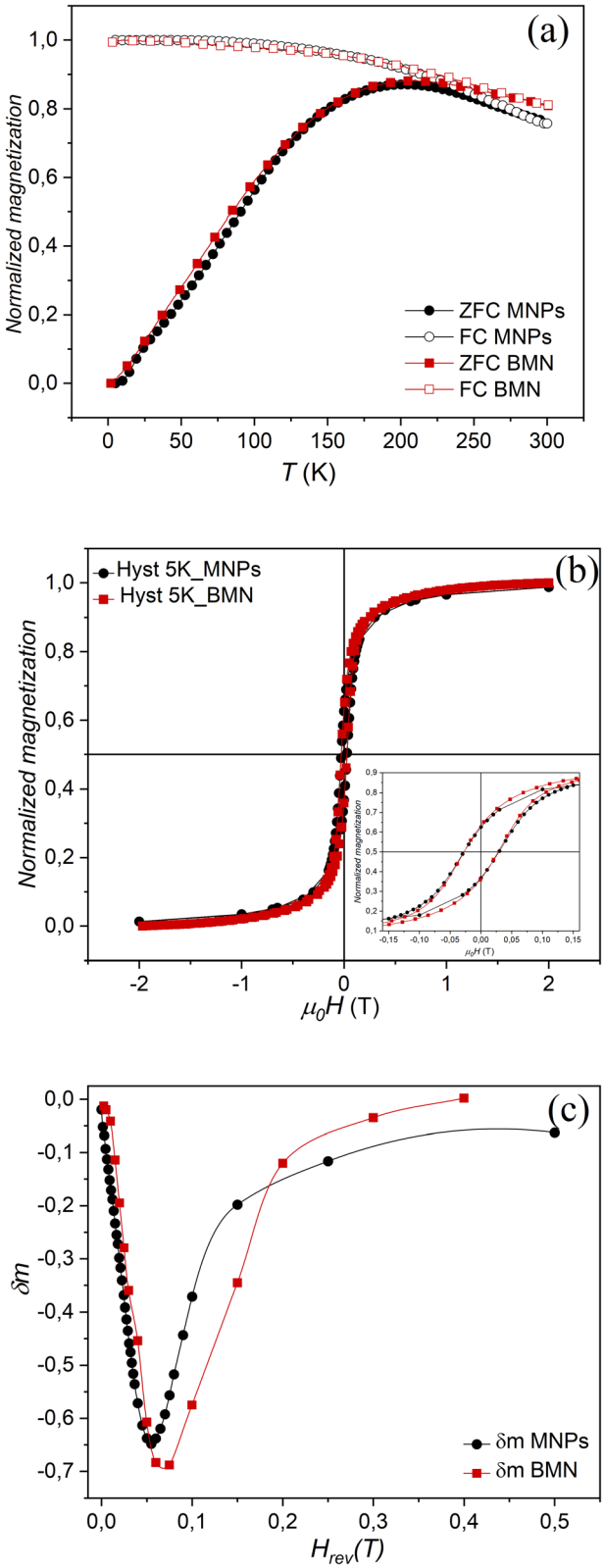

Fig. 3 (a) ZFC (full symbols) and FC (empty symbols) curve measured at 2.5 mT, (b) *M vs. H* curves recorded at 5 K, inset give details around zero field, and (c) δ_m plots for MNPs and BMN samples; in all graph MNPs are indicated by circles and BMN by squares.

Table 1 Temperature corresponding to the maximum in ZFC curve (T_{max}), irreversibility temperature (T_{irr}), mean blocking temperature ($\langle T_b \rangle$); saturation magnetization (M_s), reduced remanent magnetization (M_r/M_s), coercive field ($\mu_0 H_c$)[a]

Sample	T_{max} (K)	$\langle T_b \rangle$ (K)	T_{irr} (K)	M_s (A m^2 kg^{-1})	M_r/M_s	$\mu_0 H_C$ (T)
MNPs	202(6)	100(3)	273(8)	77(3)	0.27(2)	0.028(3)
BMN	214(6)	82(2)	221(6)	69 (3)	0,28(2)	0.027(3)

[a] Uncertainties in the last digit are given in parentheses.

samples within experimental error (Table 1). The blocking temperature (T_b) is defined as the temperature at which the relaxation time equals the timescale of the experimental technique. T_b is proportional to the anisotropy energy barrier ($E_a = KV$), and due to the distribution in volume of real MNPs systems a distribution of T_b is always present. In this scenario, the mean blocking temperature ($\langle T_b \rangle$) is typically defined as the temperature at which 50% of the particles exhibit superparamagnetic behavior, identifying the temperature at which 50% of the particles overcome their anisotropy energy barriers.[36] Moreover, there is a noticeable irreversible magnetic behavior between the ZFC and FC curves. The temperature at which this divergence occurs, T_{irr}, is associated with the blocking temperature of the largest particles.[35] T_{irr} is determined as the point where the difference between M_{FC} and M_{ZFC} drops below 3%.[37,38] As the temperature decreases, the FC curves display a plateau-like shape, indicating the presence of strong interparticle interactions within both samples. MNPs and BMN samples show small difference in values of T_{max}, T_{irr} and $\langle T_b \rangle$ (Table 1) suggesting that CaLB functionalization does have negligible influence in magnetization dynamics of nanoparticles.

Field dependence of magnetization was analyzed at 5 K and 300 K, and when irreversibility is observed the hysteresis parameters, such as saturation magnetization (M_s), coercive field ($\mu_0 H_c$), and reduced remanent magnetization (M_r/M_s), were extracted from the *M vs. H* curves and are presented in Table 1. At 5 K (Fig. 3b), the hysteresis loop shows low values of M_r/M_s and H_c, as expected for spinel iron oxide nanoparticles.[39] Using the LAS equation, an M_s value of 77(3) A m^2 kg^{-1} was obtained for bare MNPs, which is close to the bulk value (~90 emu g^{-1}).[40] The M_s value for the BMN sample was the same within the experimental error, clearly indicating that the presence of the enzyme does not affect the magnetic features of the MNPs. This result is quite interesting because the presence of a molecular coating and its interactions with the nanoparticle surface can typically induce significant variations in M_s, magnetic anisotropy (*i.e.*, H_c and M_r/M_s).[41,42]

The effect of interparticle interactions was studied using direct current demagnetization (DCD) and isothermal remanent magnetization (IRM) protocols at 5 K (ref. 43) (ESI for details, Fig. S8†). For non-interacting single-domain particles with uniaxial anisotropy, where the magnetization reversal occurs by coherent rotation, the IRM and DCD are related through the following eqn (1):[44]

$$m = m_{DCD}(H) - 1 + 2m_{IRM}(H) \quad (1)$$

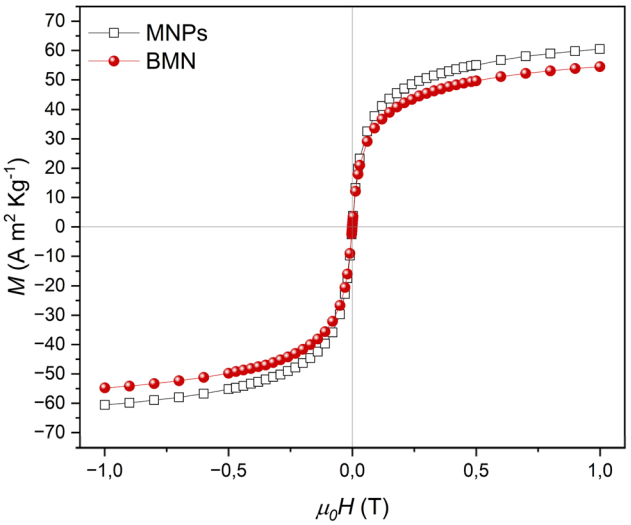

Fig. 4 Field dependence of magnetization for MNPs (empty squares) and BMN (full circles) recorded at 300 K.

In this equation, $m_{DCD}(H)$ and $m_{IRM}(H)$ represent the normalized remanence values $M_{DCD}(H)/M_{DCD}(H_{max})$ and $M_{IRM}(H)/M_{IRM}(H_{max})$, respectively, with $M_{DCD}(H_{max})$ and $M_{IRM}(-H_{max})$ being the saturation remanence magnetization. Typically, a positive peak in the δ_m plot indicates the prevalence of magnetizing interactions (*i.e.*, exchange interactions) among nanoparticles; conversely, a negative peak suggests the presence of demagnetizing interactions (*i.e.*, dipole–dipole interactions). As expected, the δ_m plots of both samples (Fig. 3c) shows the dominance of dipole–dipole interactions, with similar interaction strengths observed within experimental error. Being dipolar strength inverse proportional to the interparticle distance, this further supports that the presence of CaLB do not significant influence the morphological properties of our system.

As shown by ZFC-FC, field dependence of magnetization at 300 K (Fig. 4) confirm that both samples exhibit superparamagnetic behavior (*i.e.*, $H_c = 0$ and $M_r = 0$), with similar M_s values within the experimental error (*i.e.*, M_s (MNPs) $\simeq$ 61 A m^2 kg^{-1}; M_s (BMN) $\simeq$ 57 A m^2 kg^{-1}. It is worth to underline that after functionalization values M_s and magnetic susceptibility remain relatively high, ensuring good performance of the materials for magnetic recovery purpose.

3.2 Polycondensation

The immobilized enzyme preparation was tested for polyesters synthesis reactions. The progression of the reaction was monitored *via* ^{1}H-NMR and GPC. By analyzing the ^{1}H-NMR results (Fig. 5), it was possible to observe a monomer conversion of 92%, monitoring the intensity reduction of the signal at 3.6 ppm (disappearance of the –OCH$_3$ group of the diester due to the release of MeOH as by-product) in the ^{1}H-NMR spectra of the polymerization products together with the intensification of the signal at 4.1 ppm (–CH$_2$–O–C=O). This does not occur in a control test when the polycondensation reaction is performed

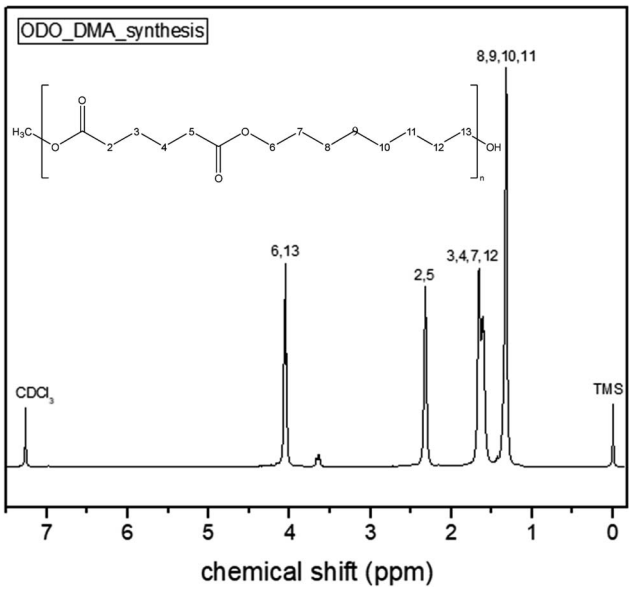

Fig. 5 ^{1}H-NMR spectra of poly(1,8-octylene adipate) synthesized using dimethyl adipate (DMA) and 1,8-octanediol (ODO) as building blocks.

using only bare MNPs. As visible in Fig. S9,† no signal reduction was observed at 3.6 ppm since the –OCH_3 group of the diester does not disappear and –CH_2–O–C═O is not formed as a demonstration of the unsuccessful synthesis of the final polyester with just 6% of monomer conversion.

Other important properties of the synthetized polyester, such as a number average molecular weight (M_n) of 5600 Da and a degree of polymerization (DP) of ∼20 were obtained from GPC analysis.

3.3. Enzymatic recyclability

In line with the principles of green and sustainable development, a long lifespan and easy recyclability are crucial for the practical application of catalysts in industry. In liquid media reactions, a rapid and efficient separation method is essential to remove the catalyst, allowing for its repeated recycling. Therefore, the chosen separation process should minimize time and energy consumption. In this context, magnetic separation (MS, *i.e.*, to use an external magnet separating magnetic catalysts from the reaction mixture) has recently gained attention as an effective alternative to traditional methods such as filtration and centrifugation. Such a method offers advantages in terms of speed, simplicity, and overall efficiency, making it both economically and technically viable with minimal catalyst loss. Additionally, magnetic separation aligns with green chemistry principles by reducing secondary waste and lowering energy requirements. Accordingly, the efficiency of MS of the BMN under investigation has been evaluated. After the reaction, the biocatalyst was recovered using an external magnetic field, washed, and reused for three cycles (Fig. S10 in ESI†). Field dependence of magnetization of BMN after each cycle has been measured at 300 K (Fig. S11a ESI†). A decrease of M_s (Fig. 6a, black full circles) has been observed with the increase of cycles indicating an increasing quantity of polyester remain attached to the MNPs. A rough estimation of the percentage of polyester has been determined by eqn (1) and reported in Fig. 6a (red empty squares). After the first cycle a quantity of polyester equal to ∼20% of the initial weight stayed attached to BMN allowing a better performance of the catalyst in the subsequence cycles as the polyester chains from the previous cycle might work as nucleation points that help the kickstart of the new reaction cycle. The percentage of polyester slightly increase in the 2nd and 3rd cycles.

Field dependence of magnetization has been investigated also on the polyester after each cycle (see ESI Fig. S11b†) showing a diamagnetic trend with a susceptibility that, as expected, is decreasing with the increasing of cycles (see ESI Fig. S11c†). All the magnetization curves have been corrected for the diamagnetic contribution (see ESI Fig. S11d†) and using the trend of M_s, the percentage of MNPs in polyester has been calculated by eqn (1). The M_s decrease with the increase of cycles number indicating a reduced percentage of MNPs, decreasing from 0.009% to 0.006% from 1 to the 3 cycle (Fig. 6b).

^{1}H-NMR and GPC were used to monitor the % of monomer conversion and the molecular weights (M_n & M_w) of the obtained

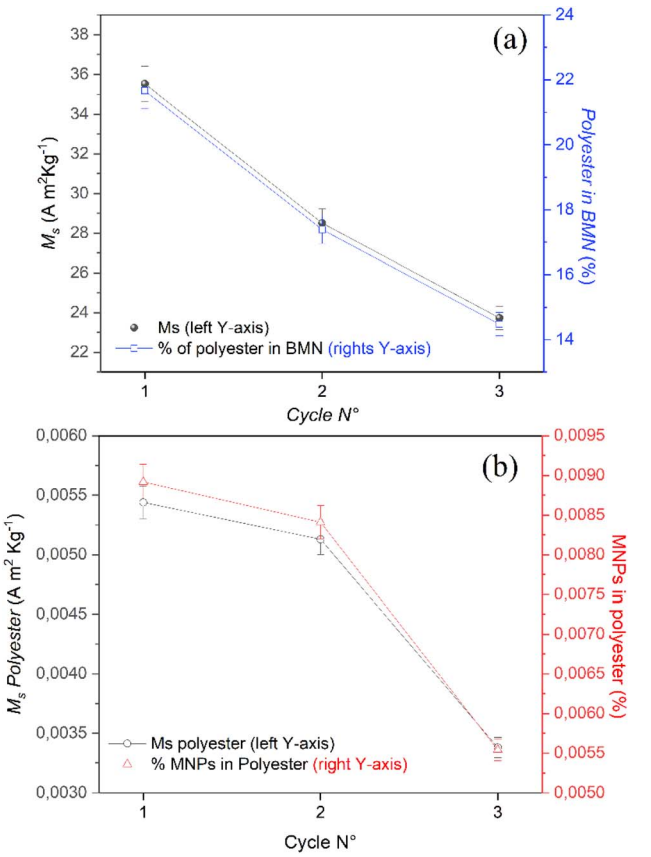

Fig. 6 Recovery of the biocatalyst: (a) M_s of BMN and % polyester in BMN after each cycle; (b) M_s of polyester and % BMN in polyester after each cycle.

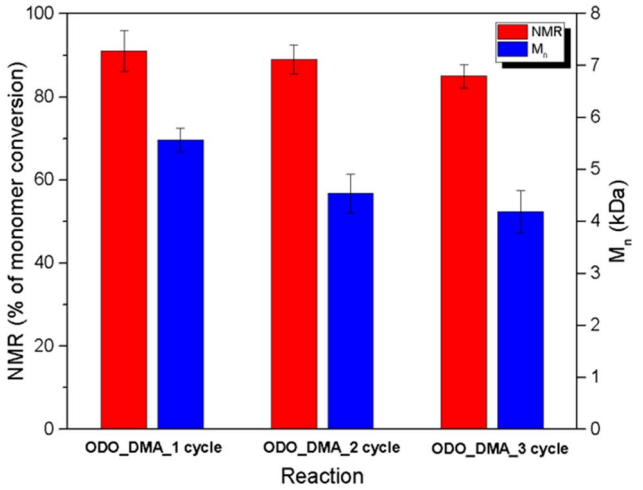

Fig. 7 Enzyme recyclability for 3 cycles of polycondensation reactions: progression of reactions was monitored *via* ^{1}H-NMR (monomers conversion, red bars) and GPC (obtained number average molecular weight, blue bars).

polyesters. As visible in Fig. 7, through the recovery of the biocatalyst *via* the application of a permanent magnet, CaLB bound magnetic nanoparticles has retained its activity over several cycles of reaction; the % of monomer conversion was found to be of 89% for the 2nd cycle and 87% for the 3rd cycle, therefore being consistent with the 92% of the 1st reaction cycle. For what concerns GPC analysis, the M_n of 5600 Da obtained for the 1st cycle was higher than the M_n of 4400 Da and 4200 Da for the 2nd and 3rd cycle respectively (~25% M_n reduction) (Table S1†). The monitored ^{1}H-NMR spectra and GPC charts of polycondensation progress over 3 cycles of reaction is reported in ESI (Fig. S12).† Hence, as it is reported in the Fig. 7, it was verified, in addition to what was previously proven by the literature on different CaLB immobilized preparations,[26,27] that BMN maintain an excellent selectivity towards long-chain diols and dicarboxylic acids for multiple reaction cycles, exploiting good recyclability due to the retainment of the enzyme's activity able to ensure high monomer conversion rate in polycondensation reactions.

Conclusion and future perspective

CaLB was successfully immobilized onto magnetic nanoparticles synthesized by co-precipitation method and enzyme recyclability was tested using dimethyl adipate and 1,8-octanediol as building blocks for biocatalyzed synthesis of polyesters.

Results showed an efficient recyclability over three reaction cycles able to ensure high monomer conversion rate and molecular weights of polyesters; in fact, the tuning of magnetic properties, achieved through the control of primary nanoparticle size, ensures efficiently magnetic recovering of the catalyst (they can be easily separated from the products by an ordinary magnetic device) and their reusability for several reaction cycles. With this paper, the authors want to underline how this not only could enhance the sustainability of enzymatic processes with environmentally friendly processes (since toxic catalysts and organic solvents are avoided) but also contributes to cost-effectiveness and scalability in industrial applications.

Data availability

The data supporting this article have been included as part of the ESI.†

Author contributions

F. P. synthesized and characterized the MNPs and carried out the synthesis experiments. F. P. and F. F. immobilized and characterized the enzyme. A. P. and G. M. G. planned the synthesis experiments. F. P. and SS wrote the manuscript. SS and DP, planned, carried out and elaborate the magnetic measurements. All authors corrected and reviewed the manuscript. A. P. and D. P. acquired the funding, designed and supervised the work. All authors have read and agreed to the published version of the manuscript.

Conflicts of interest

The authors declare no competing financial interests.

Acknowledgements

A. P. thanks the Department of Chemistry and Industrial Chemistry of the University of Genova for the Mini Curiosity Driven funding (project code: 100019-2022-AP-DIP_MINI_CURIOSITY_DRIVEN). DP and SS the Project funded under the National Recovery and Resilience Plan (NRRP), Mission 4 Component 2 Investment 1.3 – Call for tender No. 1561 of 11.10.2022 of Ministero dell'Università e della Ricerca (MUR); funded by the European Union – NextGenerationEU Award Number: Project code PE0000021, Concession Decree No. 1561 of 11.10.2022 adopted by Ministero dell'Università e della Ricerca (MUR), CUP D33C22001330002-Project title "Network 4 Energy Sustainable Transition – NEST".

References

1 J. A. Tao and R. J. Kazlauskas, *Biocatalysis for Green Chemistry and Chemical Process Development*, Wiley Online Library, 2011.
2 A. Pellis, S. Cantone, C. Ebert and L. Gardossi, Evolving biocatalysis to meet bioeconomy challenges and opportunities, *New Biotechnol.*, 2018, **40**, 154–169.
3 A. Illanes, A. Cauerhff, L. Wilson and G. R. Castro, Recent trends in biocatalysis engineering, *Bioresour. Technol.*, 2012, **115**, 48–57.
4 S. Kobayashi, H. Uyama and S. Kimura, Enzymatic Polymerization, *Chem. Rev.*, 2001, **101**(12), 3793–3818.
5 S. Kobayashi and A. Makino, Enzymatic Polymer Synthesis: An Opportunity for Green Polymer Chemistry, *Chem. Rev.*, 2009, **109**(11), 5288–5353.

6 A. Pellis, E. Herrero Acero, L. Gardossi, V. Ferrario and G. M. Guebitz, Renewable building blocks for sustainable polyesters: new biotechnological routes for greener plastics, *Polym. Int.*, 2016, **65**(8), 861–871.
7 R. A. Sheldon, Enzyme Immobilization: The Quest for Optimum Performance, *Adv. Synth. Catal.*, 2007, **349**(8–9), 1289–1307.
8 U. Hanefeld, L. Gardossi and E. Magner, Understanding enzyme immobilisation, *Chem. Soc. Rev.*, 2009, **38**(2), 453–468.
9 H. Vaghari, H. Jafarizadeh-Malmiri, M. Mohammadlou, A. Berenjian, N. Anarjan, N. Jafari, *et al.*, Application of magnetic nanoparticles in smart enzyme immobilization, *Biotechnol. Lett.*, 2016, **38**(2), 223–233.
10 S. A. Ansari and Q. Husain, Potential applications of enzymes immobilized on/in nano materials: A review, *Biotechnol. Adv.*, 2012, **30**(3), 512–523.
11 R. Jin, The impacts of nanotechnology on catalysis by precious metal nanoparticles, *Nanotechnol. Rev.*, 2012, **1**(1), 31–56.
12 L. H. Reddy, J. L. Arias, J. Nicolas and P. Couvreur, Magnetic Nanoparticles: Design and Characterization, Toxicity and Biocompatibility, Pharmaceutical and Biomedical Applications, *Chem. Rev.*, 2012, **112**(11), 5818–5878.
13 R. A. Sheldon and S. van Pelt, Enzyme immobilisation in biocatalysis: why, what and how, *Chem. Soc. Rev.*, 2013, **42**(15), 6223–6235.
14 F. Papatola, S. Slimani, D. Peddis and A. Pellis, Biocatalyst immobilization on magnetic nano-architectures for potential applications in condensation reactions, *Microb. Biotechnol.*, 2024, **17**(6), e14481.
15 L. Vaillant, S. Andresz and T. Schneider. *Environmental Impacts Associated with Radioactive Waste Management: A Review of Standards and Practices According To The Do Not Significant Harm Approach Of The European Taxonomy. Report No. 326*, 2020, available from: **https://inis.iaea.org/search/search.aspx?orig_q=RN:51056867**.
16 S. Sementsov and A. Golysheva, Green Finance in Eurasian Union: Should We Expect a Common Solution?, In *Global Challenges of Climate Change*, ed. T. C. Devezas, J. C. C. Leitão, Y. Yegorov and D. Chistilin, Springer International Publishing, Cham, 2023, pp. 223–250.
17 M. Bilal, Y. Zhao, T. Rasheed and H. M. Iqbal, Magnetic nanoparticles as versatile carriers for enzymes immobilization: A review, *Int. J. Biol. Macromol.*, 2018, **120**, 2530–2544.
18 M. I. Kim, J. Shim, T. Li, J. Lee and H. G. Park, Fabrication of Nanoporous Nanocomposites Entrapping Fe_3 O_4 Magnetic Nanoparticles and Oxidases for Colorimetric Biosensing, *Chem.–Eur. J.*, 2011, **17**(38), 10700–10707.
19 H. J. Cheon, M. D. Adhikari, M. Chung, T. D. Tran, J. Kim and M. I. Kim, Magnetic Nanoparticles-Embedded Enzyme-Inorganic Hybrid Nanoflowers with Enhanced Peroxidase-Like Activity and Substrate Channeling for Glucose Biosensing, *Adv. Healthcare Mater.*, 2019, **8**(9), 1801507.
20 M. Yang, Y. Guan, Y. Yang, T. Xia, W. Xiong, N. Wang, *et al.*, Peroxidase-like activity of amino-functionalized magnetic nanoparticles and their applications in immunoassay, *J. Colloid Interface Sci.*, 2013, **405**, 291–295.
21 A. M. Abu-Dief and S. M. Abdel-Fatah, Development and functionalization of magnetic nanoparticles as powerful and green catalysts for organic synthesis, *Beni-Suef Univ. J. Basic Appl. Sci.*, 2018, **7**(1), 55–67.
22 C. C. Yu, Y. Y. Kuo, C. F. Liang, W. T. Chien, H. T. Wu, T. C. Chang, *et al.*, Site-Specific Immobilization of Enzymes on Magnetic Nanoparticles and Their Use in Organic Synthesis, *Bioconjugate Chem.*, 2012, **23**(4), 714–724.
23 K. Khoshnevisan, A. K. Bordbar, D. Zare, D. Davoodi, M. Noruzi, M. Barkhi, *et al.*, Immobilization of cellulase enzyme on superparamagnetic nanoparticles and determination of its activity and stability, *Chem. Eng. J.*, 2011, **171**(2), 669–673.
24 S. L. Hosseinipour, M. S. Khiabani, H. Hamishehkar and R. Salehi, Enhanced stability and catalytic activity of immobilized α-amylase on modified Fe3O4 nanoparticles for potential application in food industries, *J. Nanopart. Res.*, 2015, **17**(9), 382.
25 A. Douka, S. Vouyiouka, L. M. Papaspyridi and C. D. Papaspyrides, A review on enzymatic polymerization to produce polycondensation polymers: The case of aliphatic polyesters, polyamides and polyesteramides, *Prog. Polym. Sci.*, 2018, **79**, 1–25.
26 A. Pellis, J. W. Comerford, A. J. Maneffa, M. H. Sipponen, J. H. Clark and T. J. Farmer, Elucidating enzymatic polymerisations: Chain-length selectivity of Candida antarctica lipase B towards various aliphatic diols and dicarboxylic acid diesters, *Eur. Polym. J.*, 2018, **106**, 79–84.
27 A. Mahapatro, A. Kumar, B. Kalra and R. A. Gross, Solvent-Free Adipic Acid/1,8-Octanediol Condensation Polymerizations Catalyzed by *Candida antartica* Lipase B, *Macromolecules*, 2004, **37**(1), 35–40.
28 S. Slimani, C. Meneghini, M. Abdolrahimi, A. Talone, J. P. M. Murillo, G. Barucca, *et al.*, Spinel iron oxide by the co-precipitation method: Effect of the reaction atmosphere, *Appl. Sci.*, 2021, **11**(12), 5433.
29 A. H. Morrish and R. L. Weber, The Physical Principles of Magnetism, *Phys. Today*, 1967, **20**(2), 78.
30 H. Wang, Y. Zhang, W. Yue, J. Liang and W. Su, Application of magnetic field (MF) as an effective method to improve the activity of immobilized Candida antarctica lipase B (CALB), *Catal. Sci. Technol.*, 2022, **12**(17), 5315–5324.
31 W. A. Dollase, Solid state chemistry and its applications by A. R. West, *Acta Crystallogr., Sect. B*, 1985, **41**(6), 454–455.
32 X. Xing, J. Q. Jia, J. F. Zhang, Z. W. Zhou, J. Li, N. Wang, *et al.*, CALB immobilized onto magnetic nanoparticles for efficient kinetic resolution of racemic secondary alcohols: long-term stability and reusability, *Molecules*, 2019, **24**(3), 490.
33 J. Li, X. Shi, X. Qin, M. Liu, Q. Wang and J. Zhong, Improved lipase performance by covalent immobilization of Candida antarctica lipase B on amino acid modified microcrystalline cellulose as green renewable support, *Colloids Surf., B*, 2024, **235**, 113764.

34 D. Yu, X. Zhang, T. Wang, H. Geng, L. Wang, L. Jiang, *et al.*, Immobilized Candida antarctica lipase B (CALB) on functionalized MCM-41: Stability and catalysis of transesterification of soybean oil and phytosterol, *Food Biosci.*, 2021, **40**, 100906.
35 J. L. Dormann, D. Fiorani and E. Tronc. Magnetic Relaxation in Fine-Particle Systems, In: *Advances in Chemical Physics*, John Wiley & Sons, Ltd, 1997, pp. 283–494.
36 M. F. Hansen and S. Mørup, Estimation of blocking temperatures from ZFC/FC curves, *J. Magn. Magn. Mater.*, 1999, **203**(1–3), 214–216.
37 M. F. Hansen and S. Mørup, Models for the dynamics of interacting magnetic nanoparticles, *J. Magn. Magn. Mater.*, 1998, **184**(3), L262–L274.
38 L. Del Bianco, D. Fiorani, A. M. Testa, E. Bonetti, L. Savini and S. Signoretti, Magnetothermal behavior of a nanoscale Fe/Fe oxide granular system, *Phys. Rev. B:Condens. Matter Mater. Phys.*, 2002, **66**(17), 174418.
39 G. Muscas, F. Congiu, G. Concas, C. Cannas, V. Mameli, N. Yaacoub, *et al.*, The Boundary Between Volume and Surface-Driven Magnetic Properties in Spinel Iron Oxide Nanoparticles, *Nanoscale Res. Lett.*, 2022, **17**(1), 98.
40 G. Muscas, G. Concas, C. Cannas, A. Musinu, A. Ardu, F. Orrù, *et al.*, Magnetic Properties of Small Magnetite Nanocrystals, *J. Phys. Chem. C*, 2013, **117**(44), 23378–23384.
41 D. Peddis, C. Cannas, A. Musinu, A. Ardu, F. Orrù, D. Fiorani, *et al.*, Beyond the Effect of Particle Size: Influence of $CoFe_2O_4$ Nanoparticle Arrangements on Magnetic Properties, *Chem. Mater.*, 2013, **25**(10), 2005–2013.
42 M. Abdolrahimi, M. Vasilakaki, S. Slimani, N. Ntallis, G. Varvaro, S. Laureti, *et al.*, Magnetism of nanoparticles: Effect of the organic coating, *Nanomaterials*, 2021, **11**(7), 1787.
43 S. Laureti, G. Varvaro, A. M. Testa, D. Fiorani, E. Agostinelli, G. Piccaluga, *et al.*, Magnetic interactions in silica coated nanoporous assemblies of CoFe2O4 nanoparticles with cubic magnetic anisotropy, *Nanotechnol.*, 2010, **21**(31), 315701.
44 E. P. Wohlfarth, Relations between different modes of acquisition of the remanent magnetization of ferromagnetic particles, *J. Appl. Phys.*, 1958, **29**(3), 595–596.